ULTRA SONO GRAPHY

Principles of Doppler ultrasound and emerging blood flow imaging

Dong-Guk Paeng[1]*, Cheong-Ah Lee[1,2]*, Cynthia Imtiaz[1]

[1]Department of Ocean System Engineering, Jeju National University, Jeju; [2]Center of Medicine Platform Based on Smart HemoDynamic Index (SHDI), Seoul, Korea

REVIEW ARTICLE

https://doi.org/10.14366/usg.25152
eISSN: 2288-5943
Ultrasonography 2025;44:409-424

Doppler ultrasound is one of the oldest modalities for measuring and visualizing blood flow. This review paper explores the principles of Doppler ultrasound and blood flow imaging. Following a brief history of Doppler ultrasound, all Doppler modes, including B-Flow imaging, are discussed, with emphasis on spectral broadening and Doppler spectrum amplitude in relation to clinical implications. The paper also outlines sources of uncertainty in Doppler flow measurement. Emerging technologies in blood flow imaging are introduced, including microvascular flow imaging without contrast agents and four-dimensional vascular imaging from a two-dimensional transducer, which have been commercialized within the past decade, as well as row-column array transducer systems, high-frame-rate imaging, and photoacoustic imaging, which remain in preclinical and research stages.

Keywords: Doppler ultrasonography; Spectral broadening; Spectral amplitude; Measurement accuracy; Blood flow visualization

Key points: A foundational overview of all Doppler modes including B-Flow imaging were covered, highlighting spectral broadening and amplitude of the Doppler spectrum with clinical implications. The factors of uncertainties in Doppler flow measurement including transverse plane measurement is explained. Emerging blood flow imaging includes microvascular flow, 4D vascular imaging, RC array systems, and photoacoustic imaging.

Received: August 11, 2025
Revised: August 27, 2025
Accepted: August 30, 2025

Correspondence to:
Dong-Guk Paeng, PhD, Department of Ocean System Engineering, Jeju National University, 10 Sancheondannam-gil, Jeju 63243, Korea

Tel. +82-64-754-3484
Fax. +82-64-751-3480
E-mail: paeng@jejunu.ac.kr

*These authors contributed equally to this work.

How to cite this article:
Paeng DG, Lee CA, Imtiaz C. Principles of Doppler ultrasound and emerging blood flow imaging. Ultrasonography. 2025 Nov;44(6):409-424.

Introduction

The Doppler ultrasound technique is one of the first modalities applied in medical ultrasound [1,2]. It continues to be widely used in current commercial systems to measure blood flow velocity in vessels. Since the introduction of the first Doppler technique in 1955 [3], Doppler modalities have advanced to enable real-time two-dimensional (2D) imaging, including color and power Doppler. However, these conventional techniques still require a deeper understanding to accurately interpret Doppler spectrograms and 2D visualization in real time. This review paper aims to highlight lesser-known aspects of spectral broadening and the grayscale amplitude of the ultrasonic Doppler spectrum, which may be useful for medical practitioners and sonographers.

A brief history of Doppler ultrasound is presented alongside related blood flow visualization techniques. The principles of Doppler ultrasound are reviewed with a particular focus on spectral broadening and the grayscale amplitude of the Doppler spectrum. Doppler ultrasound is commonly

regarded as reflecting only the frequency shift produced by flowing blood, which can be converted into blood velocity. However, the grayscale amplitude of the Doppler spectrum also contains information about blood properties and hemodynamics, which is often overlooked. Real-time 2D blood flow imaging techniques, such as color Doppler, power Doppler, and B-Flow imaging, are then summarized and compared [3,4]. These Doppler spectrum principles are linked to measurement methodologies and associated errors or uncertainties. Sources of measurement uncertainty are briefly outlined, with practical consideration of Doppler speed measurement in the transverse plane for small veins or tortuous vessels [5].

In the past decade, several emerging blood flow measurement and visualization techniques have been developed. Microvascular flow imaging (MVFI) and similar technologies have already been commercialized in ultrasound systems from manufacturers such as Samsung, Philips, Siemens, and Toshiba [6]. Another commercialized advance is real-time three-dimensional (3D) vascular imaging using a 2D matrix array transducer, introduced by Philips [6]. Additionally, preclinical technologies such as high-frame-rate imaging and photoacoustic imaging (PAI) are being investigated to visualize microvascular networks and measure slow blood flow in small-animal models [6,7].

This review paper explains Doppler spectral broadening and grayscale amplitude in terms of Doppler principles. Conventional pulsed-wave (PW) Doppler, color and power Doppler imaging, and B-Flow imaging are briefly summarized, compared, and discussed in relation to clinical applications. Transverse measurement methodology for blood flow is analyzed in the context of measurement accuracy. The final section introduces recent advances in blood flow visualization and measurement, including MVFI and real-time 3D vascular imaging systems. Additional technologies, such as row-column (RC) array transducer systems for real-time 3D blood flow, high-frame-rate imaging, and PAI for microvascular network visualization, are also discussed, with emphasis on their current status as preclinical or research systems [8,9].

A Brief History of Doppler Ultrasound Technique

The Doppler principle was first applied to detect the sounds of cardiac valvular motion and blood flow in the limbs and eye noninvasively using 3 MHz ultrasound by Japanese scholars in 1955 [1,2,10]. Satomura initially misinterpreted Doppler signals, attributing them to turbulent flow. In 1962, Kato et al. [3] demonstrated that the Doppler frequency shift was proportional to the velocity of laminar flow and that the voltage output magnitude corresponded to the number of red blood cells (RBCs). His team developed the first directional flow meter in 1966 [3,11]. However, his assumption that output voltage magnitude depended solely on the number of RBCs was only partially correct, as the magnitude is a nonlinear function influenced by hematocrit, RBC aggregation, the electronic system, and filtering [3,12].

In 1959, Franklin et al. [13] developed a PW ultrasonic flowmeter that enabled measurement at a specific sampling depth using pulse gating. The duplex imaging system, which combined PW Doppler sampling with B-mode imaging, was introduced in 1974 [14]. A decade later, color Doppler imaging modes were first commercialized for real-time visualization of blood flow in the 2D vessel lumen according to flow direction—initially by Aloka in 1984 and later by Toshiba in 1985 [11]. Power Doppler ultrasound, first described by Rubin et al. in 1994 [15], displays color representing the integrated power of Doppler signals across the frequency band within the vessel lumen. This development marked the first use of amplitude information from the Doppler spectrum rather than mean Doppler frequency shift data. Because of its higher signal-to-noise ratio (SNR), power Doppler enabled the visualization of smaller vessels compared to color Doppler or PW Doppler imaging. Another modality based on amplitude was B-Flow imaging, introduced by GE Healthcare in the late 1990s [12]. Several studies in the early 2000s reported applications of this new technique [11,16]. Unlike power Doppler, B-Flow imaging displays the amplitude of backscattered signals from flowing blood rather than integrated power. The backscattered signal strength is a complex function determined by factors such as the number of RBCs, the degree of aggregation, density, and compressibility contrasts between RBCs and plasma, and packing effects, in addition to sampling volume, filtering, and other electronic or digital processing. The grayscale intensity in B-Flow, similar to power Doppler, is primarily influenced by RBC aggregation, as will be described in a later section.

In the late 2010s, a new Doppler imaging method capable of detecting very low flow velocities in microvascular vessels without contrast agents was developed and subsequently commercialized in several ultrasound systems [17]. Over the past decade, additional blood flow imaging modalities have been introduced for both clinical and research use, including MVFI, four-dimensional (4D) vascular imaging with a 2D matrix array transducer, plane-wave high-frame-rate imaging, and PAI [12]. This brief history of the Doppler ultrasound techniques and blood flow visualization is summarized in Fig. 1.

Principles of Doppler Ultrasound, Including Uncertainty

This section reviews the principles and methodologies of Doppler

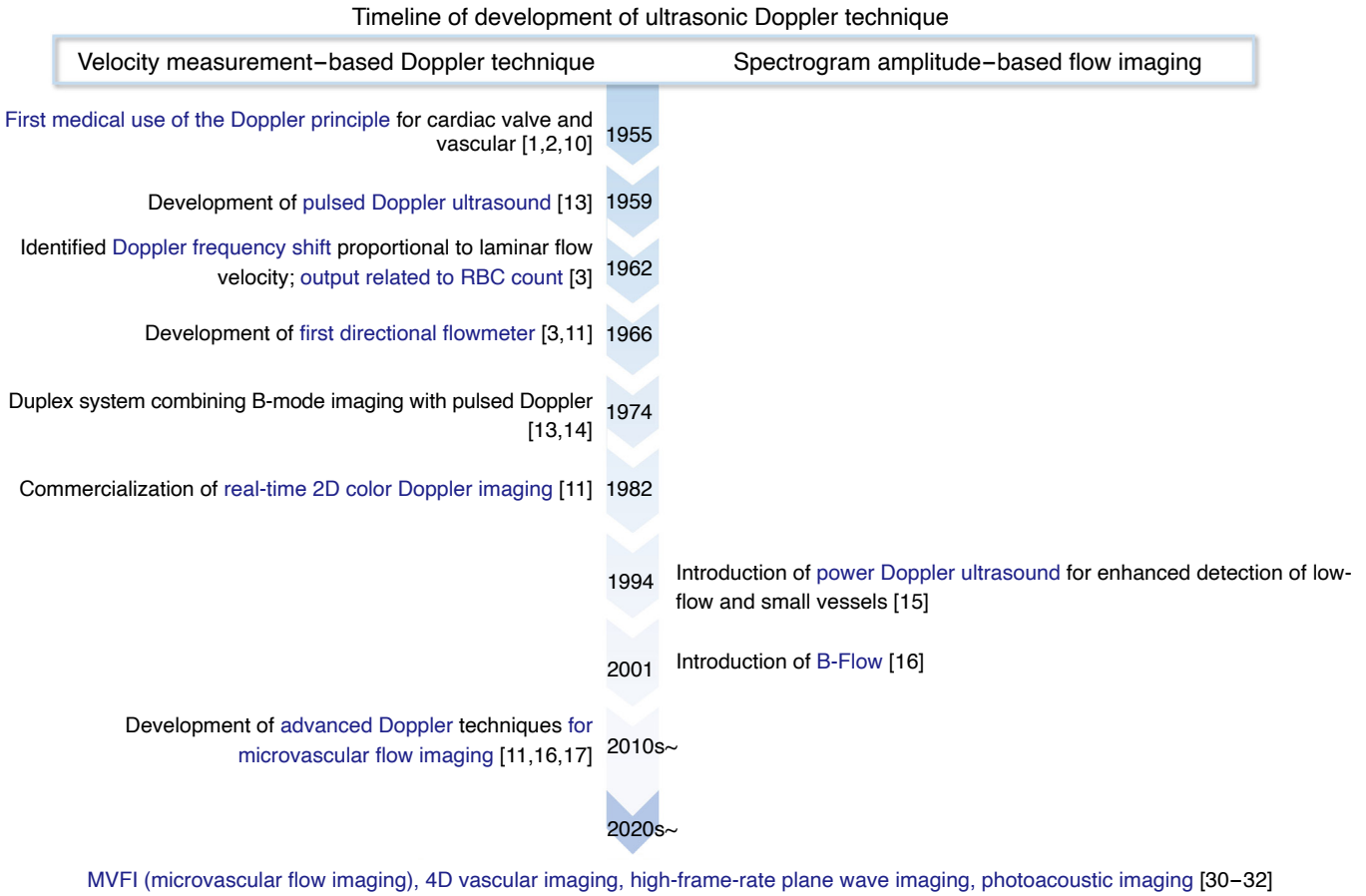

Fig. 1. **A brief history of Doppler ultrasound technology.** Satomura introduced this technology in 1955, and then Kato specified the Doppler shift for blood velocity and spectral amplitude from red blood cell (RBC) number. Other innovations include pulsed wave Doppler, color Doppler for frequency shift information, another track to use spectrum amplitude, power Doppler and B-Flow imaging, followed by emerging technologies in Doppler and blood flow imaging in the 2010s and 2020s.

ultrasound for blood flow measurement and visualization. Continuous and PW Doppler are described, with emphasis on the interpretation of Doppler frequency shifts, spectral broadening, and spectral amplitude. Color Doppler, power Doppler, and B-Flow imaging are also discussed, along with their clinical implications. The advantages and disadvantages of these Doppler techniques and blood flow visualization modalities are compared.

Doppler Principles with Continuous and PW Doppler

Doppler ultrasound enables noninvasive, real-time assessment of hemodynamics by measuring frequency shifts in ultrasound signals backscattered by moving RBCs. Two primary categories of Doppler ultrasound have been developed: continuous-wave (CW) and PW Doppler. CW Doppler employs two transducer elements, one transmitting continuously and the other simultaneously receiving backscattered signals from tissues and flowing blood. This method can capture all velocity components within vessels along the ultrasound beam path [18]. CW Doppler is particularly valuable for detecting high flow velocities, which are frequently encountered in cardiovascular diagnostics. It plays an essential role in noninvasive assessment of cardiovascular hemodynamics and has established clinical applications in conditions such as aortic valve stenosis and aortic regurgitation [19–22]. However, CW Doppler inherently lacks depth information, which limits its ability to localize flow precisely or to distinguish signals from adjacent vessels [10,17]. In contrast, PW Doppler transmits and receives short ultrasound pulses with a single transducer, providing depth-specific velocity measurements within a defined sampling volume. These measurements are widely applied for evaluating velocity and cardiac output within localized cardiac regions, assessing valvular regurgitation [23,24], estimating the degree of vascular stenosis [25–27], and quantifying pressure gradients across heart valves [5,28]. However, because PW Doppler employs a single transducer element, it is subject to a maximum measurable velocity limit [29]. Duplex imaging, which displays the sampling volume of PW Doppler on B-mode vessel images together with the Doppler spectrogram, is commonly used to quantify blood

velocity at specific vessel sites.

The fundamental principle of Doppler ultrasound is that the frequency of backscattered ultrasound waves changes proportionally to the relative motion between the transmitted wave and scatterers, typically RBCs [33]. The measured frequency shift ($\Delta f = f_0 - f_1$), where f_0 is the emitted ultrasound frequency and f_1 is the backscattered ultrasound frequency, is a function of the velocity (v) of the scatterers, incidence angle (θ) between the ultrasound beam and blood flow direction, and the sound speed (c) in blood, as expressed in the Doppler equation:

$$f_0 - f_1 = \Delta f = \frac{2v\cos\theta}{c} f_0$$

Several factors influence the measurement accuracy. Although the emitted frequency (f_0) and sound speed (c) in the blood are relatively consistent, Doppler ultrasound systems are prone to significant errors in blood flow velocity measurements. Overestimation of velocity has been reported in several studies [4]. One of the most critical factors is the angle of incidence. Additional contributors include sampling volume, signal processing, and electronic system characteristics, though these are not addressed in detail here.

As illustrated in Fig. 2, the Doppler frequency shift is greatest when the ultrasound beam is parallel to flow (0° or 180°), though this alignment is rarely achievable in practice. Optimal accuracy is generally obtained at incidence angles ≤60°. At 90°, the cosine term equals zero, producing no Doppler shift and making velocity measurement impossible. In clinical applications, PW Doppler or duplex mode typically relies on real-time determination of peak or mean blood flow velocities derived from the Doppler bandwidth. In certain cases, the Doppler frequency spectrum broadens, a phenomenon known as spectral broadening, which is explained in the next section.

Doppler Spectral Broadening

Doppler spectral broadening primarily arises from the simultaneous detection of multiple velocity components within the sample volume [34,35]. Although often misinterpreted as a sign of turbulence, it may simply reflect limitations in sampling technique. True flow disturbance or turbulence also broadens the Doppler spectrum, but additional causes include improper sampling, inappropriate gain settings, and inherent velocity differences within the sample volume. Consequently, careful attention to sampling conditions and spectral context is essential when interpreting spectral broadening in Doppler spectrograms. Misinterpretation can lead to diagnostic errors, particularly when evaluating vascular pathology or blood characteristics. Conversely, a small and accurately positioned sample volume within a laminar flow region produces a narrow, well-defined spectral envelope that faithfully represents uniform velocities.

Spectrogram and Doppler Spectral Amplitude

In ultrasonic Doppler spectra, velocity information is typically derived from the Doppler frequency shift. However, the amplitude of the Doppler spectrum—displayed as grayscale intensity in the spectrogram—also provides hemodynamic insights beyond velocity. At any given time point, the variation in grayscale amplitude

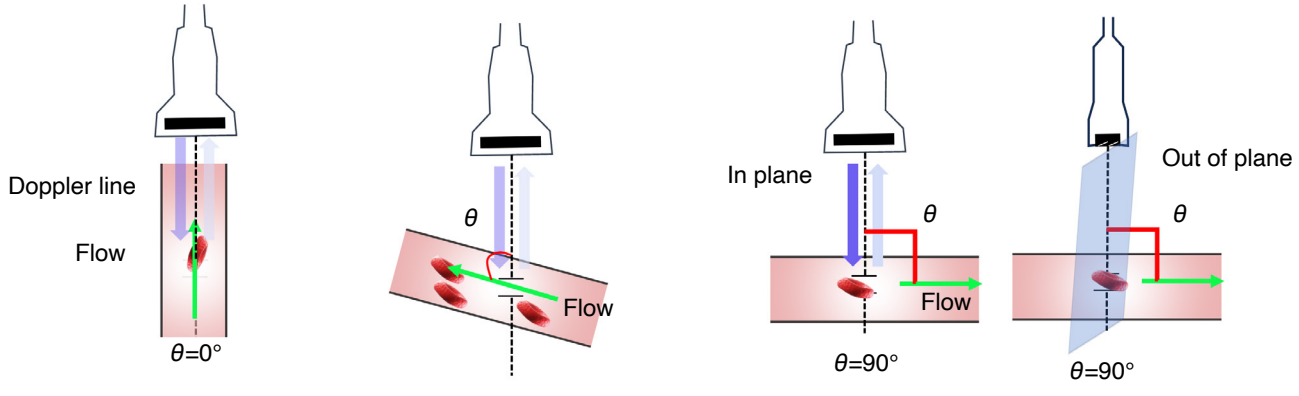

Fig. 2. Schematic illustration of the influence of the incidence angle (θ) between the ultrasound beam (Doppler line) and blood flow direction on Doppler ultrasound measurements.
A. When the ultrasound beam is parallel to the direction of blood flow (θ=0°), the maximum Doppler frequency shift is observed, although this orientation is not practical. B. At an oblique angle, the measured Doppler shift decreases according to the cosine of the angle. C. When the ultrasound beam is perpendicular to the blood flow (θ=90°), no Doppler frequency shift is detected, regardless of whether the vessel is imaged in-plane or out-of-plane.

along the frequency (y-) axis reflects the strength of backscattered ultrasound signals across the frequency band. This Doppler spectral amplitude is primarily determined by the number and size of scatterers within the sample volume, provided that other factors, such as the transducer, electronic system, and filter compensation, remain constant [36]. Fig. 3 presents PW Doppler images acquired from two different scattering media under identical conditions: an incidence angle of 60° and a sample volume of 2 mm within the same tube. Fig. 3A shows results from a viscous mixture of water, glycerol, and potato starch (2:3:0.1 by volume), while Fig. 3B depicts porcine whole blood. The most striking differences between the two media appear not only in velocity profiles but also in grayscale amplitude. In the glycerol solution, potato starch particles serve as weak scatterers, whereas in porcine whole blood, the dominant backscatter is generated by RBCs, producing a much stronger signal. Velocity differences are primarily attributable to the distinct viscosities of the two fluids, since both the pump and ultrasound system settings were unchanged.

Fig. 4A shows duplex imaging with a PW Doppler spectrogram over a pulsatile cycle. The corresponding Doppler waveform (Fig. 4B) and spectrogram (Fig. 4C) are introduced schematically. The waveform illustrates temporal variations in Doppler signal amplitude, derived from frequency shifts and amplitude changes within the sample volume. The spectrogram provides a quantitative depiction of temporal variation in both frequency shift and amplitude. Notably, the area under the frequency–amplitude curve (frequency×amplitude) represents Doppler power, which remains constant for a given scatterer population. As a result, lower-frequency components are associated with higher amplitudes and narrower bandwidths, whereas higher-frequency components produce lower amplitudes and broader bandwidths due to larger velocity fluctuations within the sample volume and the system's frequency response. Increased grayscale amplitude in low-frequency regions can also result from smaller velocity variations and system response characteristics.

Doppler spectral amplitude is determined by a combination of factors, including the electronic system, digital signal processing, and backscattering strength from flowing blood. The backscattered strength itself depends on hematocrit (RBC fraction per unit volume) and its nonlinear packing factor, the size of RBCs and rouleaux, and the acoustic impedance mismatch (density and compressibility differences) between RBCs and plasma [36]. Excluding system-related contributions, Doppler amplitude is largely governed by the strength of backscatter from blood. Under the assumption that RBCs act as Rayleigh scatterers (smaller than the ultrasound wavelength), backscattered intensity is proportional to the square of scatterer volume, a nonlinear hematocrit-dependent packing factor, the fourth power of frequency, and the square of the normalized density/compressibility difference between RBCs and plasma. Doppler power, defined as spectral amplitude integrated over the frequency bandwidth, is primarily influenced by RBC aggregation and varies within the pulsatile cycle [9]. Fig. 4D illustrates two representative hemorheological factors affecting amplitude at higher frequencies: RBC aggregation and local hematocrit changes.

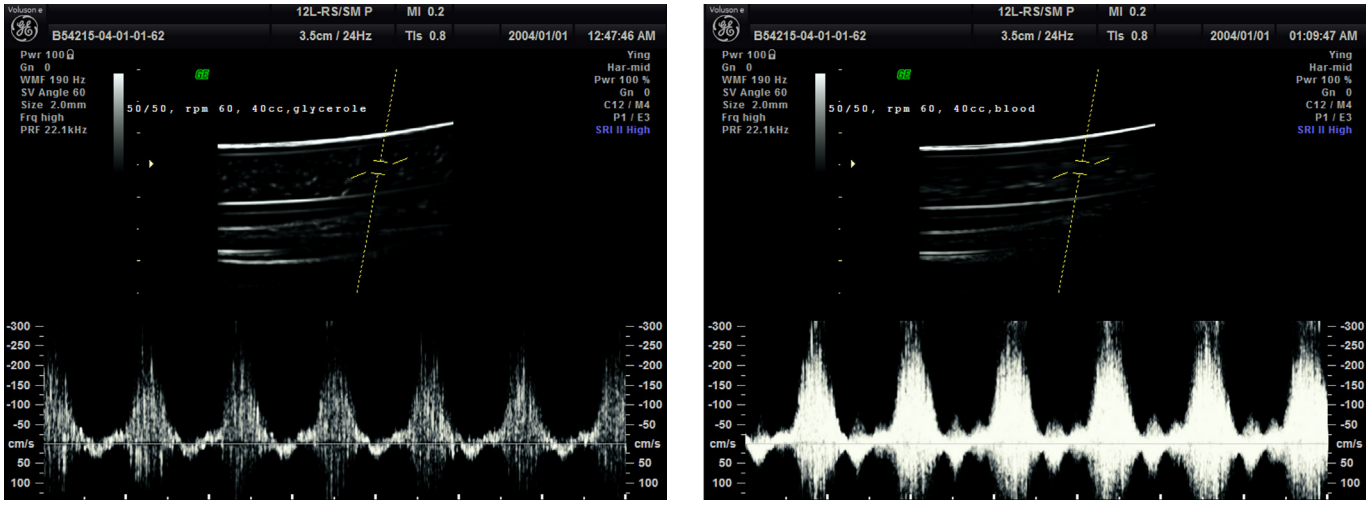

A B

Fig. 3. **Pulsed-wave (PW) Doppler images acquired from a sample with angle of 60° and a sample volume of 2 mm within the same flow tube.**

Two spectrograms show distinct differences in both velocity and grayscale amplitude. (A) PW Doppler imaging with a viscous fluid mixture and (B) porcine whole blood.

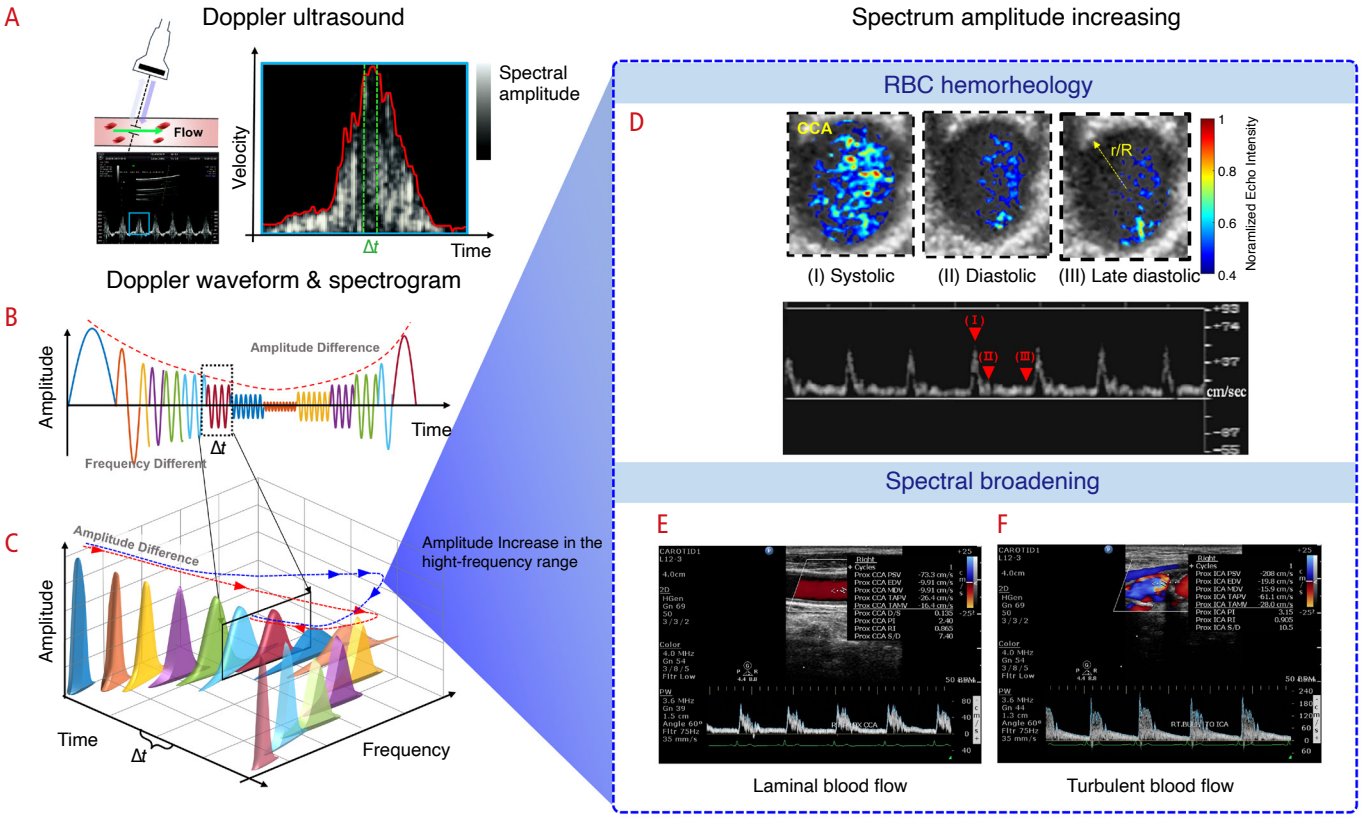

Fig. 4. Doppler waveform and spectrogram: mechanisms of spectral amplitude enhancement by hemorheology and spectral broadening. A. Schematic represents time-dependent velocity and grayscale amplitude within the Doppler sample volume based on the Doppler principle. B. Doppler waveform illustrates the composition of various frequency and amplitude components over time. C. Doppler waveform illustrates temporal changes in frequency shift and amplitude, where higher frequency components generally show decreased grayscale amplitude; however, in blood flow, amplitude at higher frequencies can increase due to hemorheological properties such as elevated hematocrit and erythrocyte aggregation. D. B-mode ultrasound image of the common carotid artery (CCA), shows that echogenicity (spectral amplitude) varies with hemorheological factors, such as cyclic changes in red blood cell (RBC) aggregation during a cardiac cycle. E. Doppler waveform acquired from the proximal CCA exhibits laminar flow characteristics. F. Doppler waveform from the internal carotid artery of a patient with greater than 70% stenosis, demonstrates turbulent flow and spectral broadening. Note that amplitude can also be affected by spectral broadening.

In particular, cyclic increases in echogenicity due to RBC aggregation under pulsatile flow have been reported previously [15]. These hemorheological processes can therefore contribute to amplitude enhancement. Thus, grayscale amplitude within the spectrogram provides indirect information on RBC concentration, aggregation dynamics, and rheological or viscosity changes [15]. Previous studies have demonstrated that arterial flow under pulsatile conditions may exhibit transient increases in Doppler power linked to RBC aggregation or localized hematocrit changes during systole, as shown in Fig. 4D [37–39]. This transient enhancement of backscattered signals—known as the "bright collapsing ring"—has been observed in Doppler power and B-mode imaging using *in vitro* porcine blood and *in vivo* human carotid and radial arteries [24,40]. This evidence suggests that analysis of Doppler spectral amplitude, reflecting the backscattered strength of flowing blood, provides valuable insights into RBC dynamics and the hemorheological properties of blood flow [41]. While quantitative clinical application of spectral amplitude remains impractical, its interpretation is essential for understanding power Doppler and B-Flow imaging.

Color Doppler and Power Doppler

Color Doppler imaging provides a directional flow-speed map using the BART convention (blue away, red toward) superimposed on B-mode vessel images. The brightness of each color corresponds to the magnitude of the Doppler frequency shift, and thus to higher flow velocities, although angle dependence can influence this relationship. This real-time 2D technique relies on autocorrelation in the time and spatial domains rather than on frequency-domain

Doppler spectral analysis, enabling rapid processing [42]. While color Doppler displays flow velocity qualitatively through color brightness, it does not yield fully quantitative velocity measurements. Quantification is generally performed using PW Doppler spectrograms in duplex imaging. Both color and PW Doppler imaging employ wall filters to eliminate low-frequency signals from tissue motion, such as pulsation and respiration. However, these filters also suppress low-velocity blood flow components, reducing sensitivity [34].

In power Doppler imaging, Doppler power—defined as the integrated spectral amplitude across the frequency band—is mapped to color brightness, independent of velocity and direction. Later developments added optional directional information. Power Doppler is less dependent on the angle of insonation and is particularly effective for small-vessel visualization due to the high SNR achieved by integrating power over the frequency range. It is reported to be approximately three times more sensitive than color Doppler [43]. This Doppler power mode provides spectral amplitude information, as explained in the previous section. Fig. 5 shows duplex color Doppler imaging (Fig. 5A) and power Doppler imaging (Fig. 5B) with a PW Doppler spectrogram, measured from a branch of the carotid artery.

Thus, color Doppler is best suited for evaluating flow direction, velocity, and turbulence, making it particularly useful for large vessels and flows with moderate-to-high velocities. By contrast, power Doppler is highly sensitive to low-velocity flow, even though it does not provide velocity magnitude or directional information. This makes it advantageous for detecting small-vessel flow, inflammatory hyperemia, tumor vascularity, and residual slow flow distal to severe stenosis [6,43]. These complementary features support their clinical application for both diagnostic evaluation and treatment monitoring. Table 1 summarizes the clinical uses and distinguishing characteristics of color and power Doppler imaging by lesion type [44–53].

B-Flow Imaging

The echoes generated by RBCs are typically ~1/1,000th the intensity of surrounding tissue signals (–60 dB), causing the vascular lumen to appear black on conventional ultrasound. Using a long transmit pulse can amplify these weak signals, but at the cost of spatial resolution, since resolution is inversely proportional to pulse length [54]. To address this, GE developed the B-Flow imaging system in the late 1990s, using digitally encoded ultrasound with tissue–blood equalization technology to suppress tissue echoes while amplifying blood signals. This approach allows backscattered blood echoes to be displayed with spatial resolution comparable to grayscale imaging. B-Flow provides real-time visualization of blood flow dynamics with high spatial and temporal resolution, free from Doppler-related artifacts such as color blooming or aliasing [55]. Although it does not directly provide velocity or directional information, it produces clearer vascular and flow images than conventional duplex ultrasound. Directional data were later incorporated in B-Flow color imaging, similar to enhancements made in power Doppler. Like power Doppler, B-Flow represents another modality that utilizes the amplitude of backscattered signals from flowing blood [56,57].

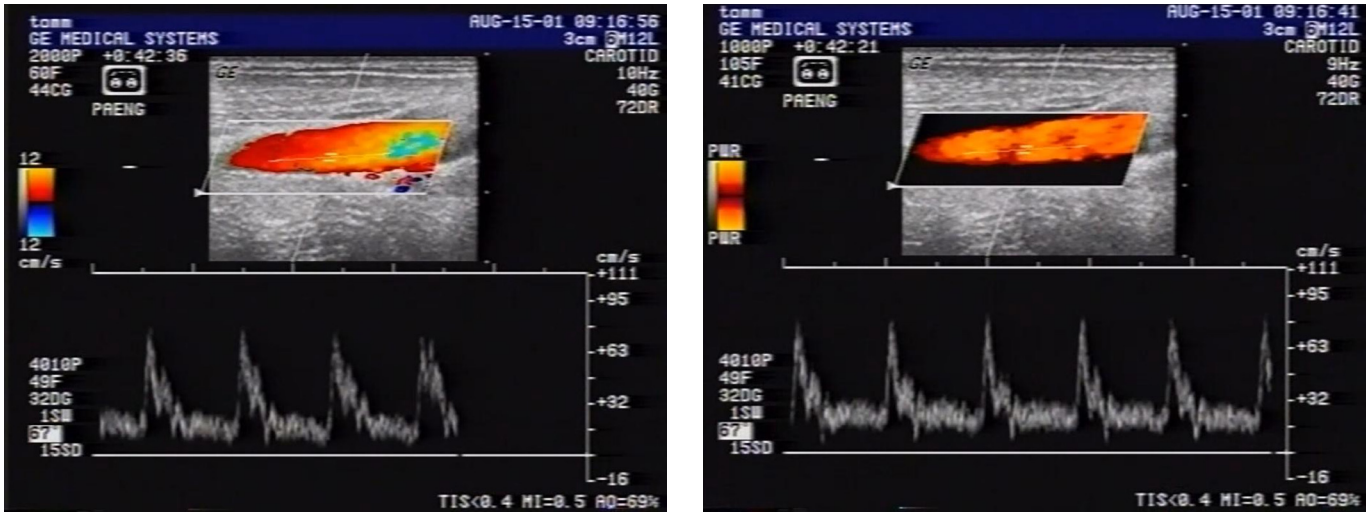

A B

Fig. 5. Duplex color and power Doppler imaging with pulsed-wave Doppler.
Duplex color Doppler (A) and power Doppler imaging (B) were performed with pulsed-wave Doppler, measured from the bifurcation of the carotid artery.

Table 1. Summary of clinical applications of color Doppler and power Doppler imaging

Lesion type	Color Doppler	Power Doppler	Reference
Stenosis/Occlusion	- Best for assessing hemodynamic severity of stenosis via flow direction and velocity; less sensitive for very slow flow	- Highly sensitive for detecting very slow or residual flow and distinguishing subtotal from complete occlusion. - No flow direction or velocity information	[7,46]
Tumorous lesions	- Provides flow direction and velocity within tumor vessels - Exhibits sensitivity for very slow or microvascular flow	- Visualizes peritumoral microvasculature and estimates vascular density - Better depiction of overall vascular density in tumors - Less affected by angle dependence - Susceptible to motion artifacts	[47–51]
Inflammatory lesions	- Differentiates arterial vs. venous flow in inflamed tissue - Enables grading of vascularity in synovitis and dermatologic inflammation - May miss early neovascularization	- Higher sensitivity for detecting low-velocity flow in inflamed tissue and synovial microvasculature - More accurate depiction of neovascularization extent - Useful for monitoring therapy response via changes in microvascularity - Does not provide flow direction or velocity - Sensitive to motion artifacts in superficial inflamed regions	[52,53]

Table 2. Comparison of five ultrasound modalities—CW and PW Doppler, color Doppler, power Doppler imaging, and B-Flow (color)—based on their underlying physics, display formats, and functional capabilities

Feature	CW Doppler	PW Doppler	Color Doppler	Power Doppler	B-Flow (color)
Doppler frequency shift	Yes	Yes	Yes	No but integrated	No
Amplitude in spectrum	No, but gray scale	No, but gray scale	No	Yes, but integrated	Yes, but in backscattered
Display spatial dimension	Spectrogram	Spectrogram	2D (blue away, red toward)	2D color	2D gray (gradient)
Directionality	Directional	Directional	Red/blue encoding	No but added	No but added in color
Velocity quantification	Velocity in whole depth	Velocity in sample	Relative only	No	No
Wall filters to remove low-velocity flow	Yes	Yes	Yes	Yes	No
Aliasing	Yes	Yes	Yes	No	No
Angle dependency	High	High	High	Minimum	No
Spatial resolution	None	Sampling depth	Bad	Bad	Good
Hemodynamics information	Directional flow velocity	Directional flow velocity	Directional flow velocity	Flow presence	Flow pattern (directional)
Penetration	Good	Good	Good	Good	Moderate
Clinical practices	Limited	Often	Often	Often for small vessels	Limited

CW, continuous wave; PW, pulsed wave.

Fig. 6 shows cross-sectional B-Flow imaging of the carotid artery acquired with a GE Healthcare LOGIQ P9 system. This modality enables high spatial-resolution visualization of temporal changes in ultrasonic echogenicity caused by RBC motion. As a result, it captures dynamic blood flow variations throughout the cardiac cycle, including both diastolic deceleration (Fig. 6A) and systolic acceleration (Fig. 6B). Although B-Flow does not provide quantitative velocity or directional data, it is particularly well suited for qualitative assessment of dynamic arterial flow patterns *in vivo*.

Overall, Table 2 highlights that CW and PW Doppler are most effective for quantitative velocity measurements, color Doppler is optimal for mapping flow direction and relative velocity, power Doppler excels at detecting the presence of low-velocity flow, and B-Flow provides high-resolution anatomical visualization without Doppler-related artifacts.

CW Doppler continuously transmits and receives ultrasound signals, allowing the detection of very high velocities without aliasing. However, it lacks depth resolution. PW Doppler, by transmitting short pulses, provides velocity measurements at specific depths, producing a spectral waveform with frequency shift and amplitude information. Its limitation lies in Nyquist aliasing at high velocities. Both CW and PW Doppler provide quantitative velocity data and precise directional information in a 1D waveform display [57,58].

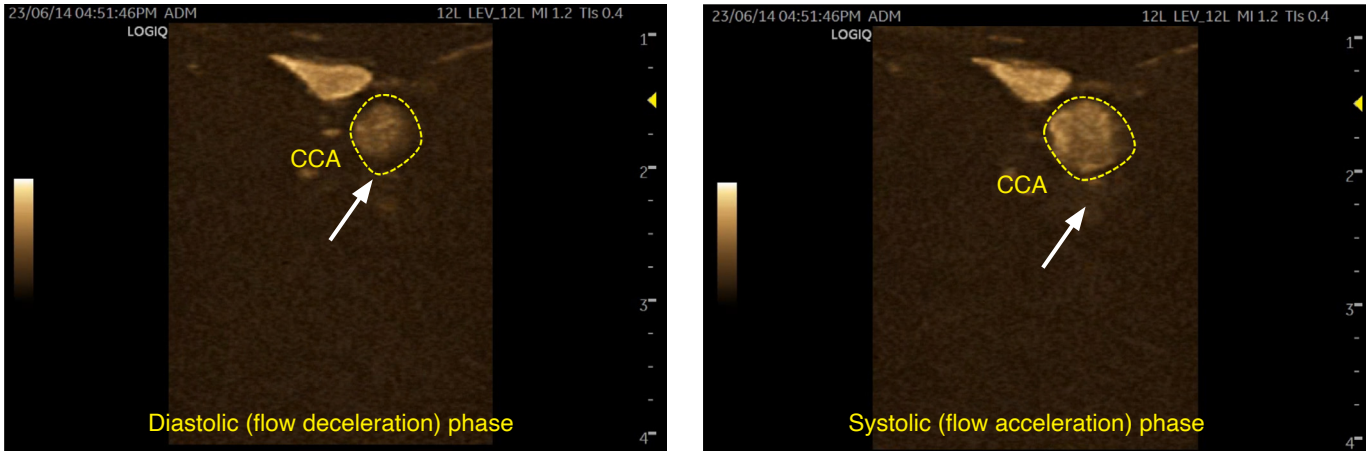

A B

Fig. 6. Cross-sectional B-Flow imaging of the common carotid artery (CCA) acquired with a GE Healthcare LOGIQ P9 system. The diastolic phase (A) and the systolic phase (B) are shown. The arrows indicate the CCA.

Color Doppler overlays 2D color maps on B-mode images to indicate the direction and relative magnitude of flow. While it provides useful anatomical context, it suffers from angle dependence, reduced spatial resolution, and aliasing at high flow velocities. Power Doppler, which maps signal amplitude rather than frequency shift, is more sensitive to slow or small-vessel flow and less susceptible to aliasing. However, it does not measure velocity, though later directional modes were introduced to visualize flow orientation [48].

B-Flow, by contrast, is a non-Doppler approach that directly visualizes moving scatterers such as RBCs in grayscale. This technique provides high-resolution imaging of both vessel walls and the lumen without aliasing or angle dependence, though it lacks velocity or hemodynamic quantification. B-Flow color extends this by adding directional color coding, thereby maintaining anatomical clarity while indicating flow direction, but still without quantitative velocity data [59].

Measurement Uncertainty from Angle and Transducer Plane

Several factors influence the accuracy of PW Doppler spectrogram measurements. These include transmitting frequency, the sound speed of the medium, and sampling volume, although their effects are relatively minor. Greater uncertainty arises from how velocity is derived from the Doppler spectrum—whether maximum or mean frequencies are used. Additional contributions to inaccuracy stem from signal processing algorithms, the frequency response function, and wall filter design. Among all sources of error, the angle between the ultrasound beam and the direction of blood flow is one of the most critical in practice. Consequently, proper alignment of the transducer with the vessel is essential for accurate velocity estimation. This section focuses on the implications of angle and transducer alignment for Doppler measurement accuracy.

When measuring blood flow velocity with Doppler ultrasound, the longitudinal view is recommended as the standard approach [60–62]. This orientation reduces uncertainty regarding the angle between the ultrasound beam and blood flow in duplex mode, although some ambiguity remains in the depiction of flow direction relative to the ultrasound beam in B-mode images. The ultrasound beam diverges outside the focal region, and sampling volume placement in duplex imaging is not always exact. Furthermore, frequency bandwidths in the spectrogram must be converted into blood velocity, introducing uncertainty depending on whether peak and/or mean frequency values are applied. Maintaining an optimal incidence angle is especially challenging in tortuous or deeply located small vessels, making measurement accuracy heavily operator-dependent. In contrast, the transverse view, while providing intuitive anatomical visualization, is generally unreliable for velocity quantification because the beam is nearly perpendicular to the flow [63]. As a result, consistency, repeatability, and reproducibility of transverse-based quantitative measurements are inadequate. To address these limitations, a phantom study investigated the feasibility of tilted transverse views. The aim was to evaluate the impact of probe tilt angle on velocity measurements in the transverse plane and to compare them with standard longitudinal measurements (Fig. 7A). Tortuous and straight vessel phantoms were fabricated using silicone tubing with an internal diameter of 2 mm (Fig. 7B). Flow velocities were recorded under defined conditions using PW Doppler, with measurements obtained at

varying probe tilting angles, as illustrated in Fig. 7C. A Bland-Altman analysis (Fig. 7D) was performed to assess agreement and bias between longitudinal (L) and tilted transverse (T) measurements. The results demonstrated agreement between longitudinal and transverse scans with probe tilts of 5°, 10°, and 15° [T(5), T(10), T(15)], with the smallest bias observed at 15° (−0.4), indicating the closest correspondence between methods. Maximum velocities were measured for two vessel types across multiple flow conditions, yielding 12 datasets for analysis. These findings suggest that tilting the probe by approximately 15° provides velocity measurements most consistent with standard longitudinal scanning. This approach may serve as a practical alternative for evaluating reflux in small and irregular veins [64], such as tortuous saphenous veins in the extremities. In situations where longitudinal scanning is technically difficult, tilting the probe by about 15° to 20° in the transverse plane may offer hemodynamic information comparable to longitudinal Doppler. However, additional studies are needed to confirm reproducibility and consistency in clinical practice. Validation of this technique would support its potential as a practical diagnostic tool for small and tortuous vessel diseases.

Emerging Blood Flow and Vessel Imaging

Two recently commercialized technologies have advanced blood flow measurement and imaging: MVFI and 4D vascular imaging using a 2D array transducer system. In addition, several preclinical and research-stage methods, such as RC array transducers, high-frame-rate plane-wave imaging, and photoacoustic imaging, are being developed for visualizing microvascular networks and measuring slow blood flow. This section briefly introduces each modality, with emphasis on their underlying principles, resolution, and clinical applications.

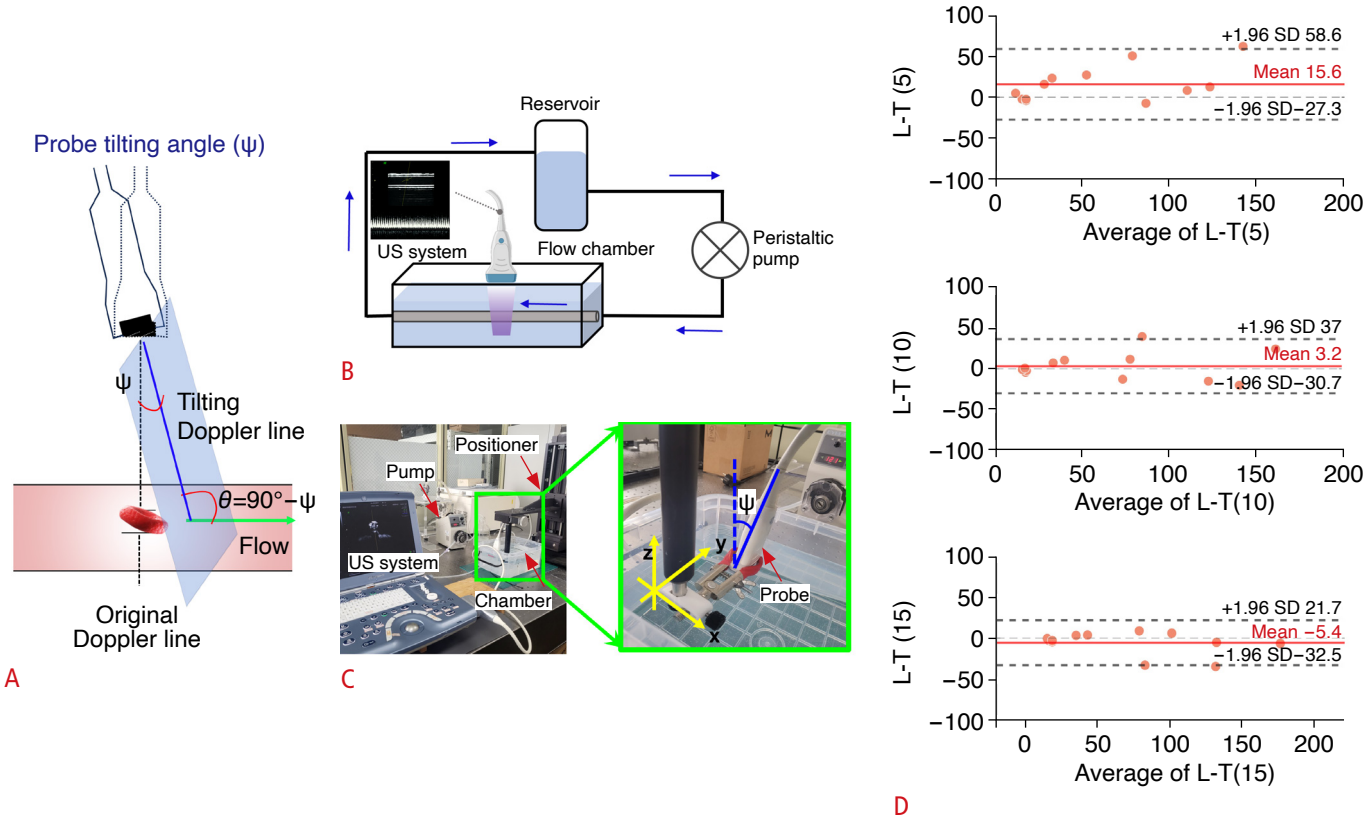

Fig. 7. *In vitro* flow phantom study for transverse and longitudinal pulsed wave (PW) Doppler measurement comparison.
A. Schematic diagram illustrates transverse PW scanning according to the tilting angle of the probe. B. Flow circulation system is used for quantitative evaluation of the feasibility. C. Experimental setup includes straight and tortuous phantom tubes. A peristaltic pump (RP-1000, Eyela, Japan) was employed to produce a consistent flow rate at 120 revolutions per minute, thereby simulating a circulatory system. PW Doppler was obtained using an ultrasound (US) imaging system (GE Voluson e, GE Healthcare, Düsseldorf/Deutschland) with a 5–13 MHz linear transducer (GE 12L-RS). D. Bland-Altman agreement analysis compares velocity measurements obtained by longitudinal and transverse PW Doppler scanning at probe tilting angles of 5°, 10°, and 15°. SD, standard deviation.

Clinical Blood Flow Imaging Systems

Microvascular flow imaging

A new Doppler-based modality was introduced about a decade ago to enhance detection of very low blood flow velocities in small vessels without the use of contrast agents. Several commercial MVFI systems are now available, including Superb Microvascular Imaging (Canon Medical), Slow Flow (Siemens Healthineers), Microvascular Imaging (GE Healthcare), MicroFlow Imaging (Philips), and MV-Flow (Samsung) [6,65]. These innovative Doppler techniques could overcome the limitations of conventional Doppler modes, which require wall filters that inadvertently remove low-velocity flow along with clutter artifacts from tissue motion. MVFI employs advanced clutter suppression techniques to isolate slow flow signals. These include spatiotemporal coherence analysis, motion suppression, artifact reduction methods, and adaptive filtering strategies such as singular value decomposition to remove clutter [6]. MVFI can also be implemented with high-frame-rate plane-wave imaging.

Clinical evidence supports the utility of this approach. In a prospective study of 30 women with fibroids (1.5–12 cm), 2D MV-Flow imaging (Samsung HERA W10) demonstrated excellent intra- and interobserver reproducibility for vascular indices and color scores (intraclass correlation coefficient, 0.992 to 0.996). MV-Flow visualized central fibroid vascularity in 63% of cases compared with only 13% using power Doppler (P=0.001) and revealed finer vascular structures. Penetration depth was also greater with MV-Flow (3.92 cm) than with power Doppler (2.95 cm, P=0.001). Consistent with broader MVFI literature, the method can detect vessels as small as ~0.5 mm in diameter and flow velocities down to ~1 mm/s without contrast enhancement. These findings suggest that MV-Flow could improve assessment of fibroid vascularity, aiding growth prediction and therapy selection [66]. Further advances include rapid, contrast-free super-resolution ultrasound using erythrocyte tracking to image human lymph node vasculature. This technique achieved sub-wavelength resolution from 2-second acquisitions, detecting vessels as small as 40 μm and flow velocities of 2–15 mm/s. It enabled reproducible visualization of vascular architecture, flow direction, and temporal dynamics, offering promise as a noninvasive tool for lymph node evaluation [67].

4D vascular imaging and blood flow quantification

In 2019, Philips commercialized the world's first 4D vascular ultrasound probe using a 2D matrix array transducer (XL14-3 xMatrix Linear Array) with 14,000 elements and a broad frequency band (3–14 MHz). This technology enables volumetric, time-resolved visualization of blood flow with unprecedented temporal and spatial resolution. The modality combines plane-wave insonification and coherent compounding with 2D matrix array transducer technology to generate full-volume blood flow data at rates exceeding 4,000 volumes per second [68]. Validation studies in phantoms and human carotid arteries demonstrated high accuracy of volumetric flow rate measurements, with errors below 5% at flow rates up to ~360 mL/min and acceptable performance even under higher flow conditions (~490 mL/min). These results confirm the feasibility of real-time hemodynamic assessment within a single heartbeat [68]. Furthermore, 4D vascular imaging can also be integrated with vector flow imaging (VFI). Together, these techniques provide high resolution, accurate velocity quantification, broad vessel size applicability, and strong clinical relevance. Reported spatial resolutions range from sub-millimeter (~0.3–0.5 mm lateral) to full-neck coverage (~10 cm) for comprehensive vascular mapping. Imaging depths extend to ~70 mm in phantom studies and cover the full carotid artery in clinical protocols. Velocity measurements range from peak systolic velocities in large arteries (e.g., 0.79±0.29 m/s at carotid bifurcations) to volumetric flow rates with <5% error under controlled conditions [59]. Vessel sizes assessed range from common carotid arteries (~6–8 mm diameter) to bilateral middle cerebral arteries and spiral phantom models [69]. Preclinical and clinical applications include carotid hemodynamic assessment [30], intracranial hemodynamic quantification, phantom validation of multidirectional pulsatile flow, and real-time visualization of complex flow fields. Multiple studies have demonstrated high accuracy in velocity and flow volume quantification, with strong agreement between ultrasound-based VFI/4D vascular imaging and 4D magnetic resonance imaging. These findings underscore the clinical potential of 4D vascular ultrasound for cerebrovascular disease evaluation and advanced flow dynamics analysis [70].

Preclinical/Research Blood Flow Imaging Systems

RC array transducer and 4D flow imaging

The RC array transducer was recently introduced to reduce to N+N elements from N×N elements for a 2D full matrix array for real-time 3D imaging, where N is the number of array elements for 1D transducer (N=128 and 64 elements for most conventional transducers and cardiac applications, respectively). Transmission occurs through row elements while reception is performed through orthogonal column elements, reducing the number of scanner connections. With appropriate multiplexing, electronic control, and high-performance GPU-based signal processing, RC arrays achieve 3D imaging quality comparable to full matrix arrays in real time. RC arrays retain most of the advantages of 2D matrix transducers, including visualization of anatomy, blood flow, tissue motion, and even super-resolution imaging with contrast agents. Unlike matrix arrays, which are impractical for large apertures, RC arrays are feasible for deeper penetration and higher sensitivity,

offering potential clinical relevance for retrospective blood flow measurements in any plane and full 3D VFI [67]. Although not yet commercialized, this technology shows strong promise for vascular and cardiac imaging [71]. One study reported a novel fabrication process for a 7-MHz, 128-element RC array using a PMN-0.28PT single crystal. Axial and lateral resolutions measured at 7.7 mm depth were ~0.20 mm and 0.41 mm, respectively. Validation on a hyperechoic phantom confirmed high-quality 3D B-mode imaging, demonstrating the array's potential for ultrafast 3D and functional ultrasound applications [72]. Another study introduced a mechanically curved RC array optimized for transthoracic cardiac imaging with a 24×16 mm^2 aperture. The toroidal array included 96 column and 64 row elements with customized curvature radii, enabling an improved field of view. Delay-and-sum beamforming with analytical wave modeling was validated through simulation and phantom experiments, achieving 3D imaging depths up to 12 cm with improved contrast-to-noise ratio. 3D Ultrasound Localization Microscopy was subsequently demonstrated on an *ex vivo* swine heart, visualizing coronary microcirculation [68,70]. *In vitro* testing of RC arrays with advanced beamforming and sub-aperture processing reduced false localization and noise by 7 dB, achieving effective frame rates >4,000 fps. *In vivo* imaging was successfully performed on a rabbit kidney and human thyroid, confirming the feasibility of high-resolution, large-field-of-view super-resolution imaging [72,73].

High frame rate imaging in Doppler ultrasound

Unlike conventional ultrasound, which relies on focused, line-by-line scanning, high-frame-rate (Ultrafast) imaging transmits plane waves that insonify a large area simultaneously. This approach allows frame rates in the thousands, exceeding 10,000 frames per second (fps) under optimal conditions. In contrast, standard B-mode and Doppler ultrasound typically operate at 30–100 fps, adequate for many applications but insufficient for phenomena such as microvascular perfusion or myocardial wall motion. In ultrafast imaging, echoes are received across all channels simultaneously and reconstructed using parallel beamforming algorithms [74]. Compounding, which refers to the rapid transmission of multiple angled plane waves (typically 3–15) followed by coherent summation, further enhances image quality. With high pulse-repetition frequencies, both tissue and flow can be imaged from the same dataset.

The integration of ultrafast imaging with Doppler modalities has enabled substantial innovations. By using the same plane-wave transmissions, B-mode and Doppler images can be co-registered. For example, reconstructions from only 10–15 beams achieve >300 fps, sufficient for cardiac wall motion analysis. Another key advantage is retrospective processing: because data from the full field are acquired simultaneously, multiple PW Doppler gates can be placed post-acquisition, allowing simultaneous velocity measurements at several vessel segments or heart chambers within a single cardiac cycle. This capability improves workflow and diagnostic efficiency [74]. Ultrafast Doppler is valuable for both large-vessel and microvascular assessment. In color Doppler, ensemble-based flow estimation benefits from ultrafast compounded sequences, which enhance wall filtering and velocity sensitivity. This is critical for detecting very slow flows (as low as 1 mm/s), such as those in tumor neovascularization or vasa vasorum imaging, where contrast use may be limited [69,74]. In vascular imaging, ultrafast frame rates enable the generation of 2D vector flow maps, providing detailed visualization of laminar and turbulent flow patterns across entire regions in real time. This capability has important clinical implications, including the assessment of atherosclerosis, valvular regurgitation, and vessel wall shear stresses—factors critical to plaque development and rupture risk. High-frame-rate imaging methods for blood flow assessment are defined by their technical specifications, equipment, and applications. Reported spatial resolutions range from the micrometer scale (~10 μm) for microvascular imaging to the millimeter scale for large-vessel evaluations. Velocity measurement capabilities extend from very slow flows (~1 mm/s in rodent cerebral microvessels) to high-velocity arterial flows exceeding 20 cm/s. Vessel size coverage spans from capillary-level microvessels (<10 μm) to large human arteries such as the abdominal aorta (~2 cm diameter) [8]. Applications include preclinical studies in transgenic and rodent models for cerebrovascular hemodynamics, microvascular network visualization, and intracranial flow quantification, as well as clinical uses in pediatric congenital heart disease, carotid atherosclerosis evaluation, aortic flow characterization, and plaque assessment. The field is trending toward high-frame-rate, vector-based, and 3D-capable imaging systems, with increasing emphasis on microvascular detection, artifact reduction, and real-time hemodynamic quantification without the use of contrast agents.

PAI for blood flow visualization

PAI has emerged over the past decade as a powerful, noninvasive, and versatile technique for visualizing biological tissues, particularly the microvasculature [31]. PAI integrates optical and acoustic methods, exploiting the strong optical absorption contrast of endogenous chromophores, such as hemoglobin, melanin, and lipids, while overcoming the resolution and penetration limits of purely optical approaches. Absorbed optical energy generates broadband ultrasonic waves, which are then detected by ultrasound transducers to reconstruct high-resolution images [33]. Because ultrasound scatters less than light in biological tissues, PAI achieves

greater penetration depth, making it suitable for multiscale imaging applications [75]. Photoacoustic microscopy, developed as a high-resolution variant, achieves sub-micrometer resolution by tightly focusing either the optical or acoustic beam. This enables imaging of microvascular networks, including individual capillaries, with exceptional detail—though at relatively shallow depths [76].

PAI has shown particular promise in neurovascular and brain imaging. Brain microcirculation, regulated through neurovascular coupling, ensures adequate blood supply to meet metabolic demand. Using PAI, researchers have visualized capillary-level hemodynamics in live rats through the intact skull, resolving vessels smaller than 10 μm at depths up to 0.6 mm [32,76]. This high resolution allows structural mapping of capillary networks as well as functional imaging through measurement of oxygen saturation gradients—key indicators of cerebral metabolism [77]. These features make PAI highly valuable for investigating neurodegenerative diseases such as Alzheimer's, where microcirculatory changes may precede structural pathology [77]. Cardiovascular imaging is another promising application. Photoacoustic tomography has been used to visualize thoracic vessels and whole-heart morphology in mice, achieving ~200 μm resolution at depths up to 10 mm [78]. In addition to structural imaging, PAI supports functional and metabolic imaging by enabling quantitative analysis of oxygen saturation levels in blood vessels. Its multispectral capability allows differentiation between oxygenated and deoxygenated hemoglobin, offering information on tissue hypoxia and ischemia without ionizing radiation [79]. Overall, PAI stands out as a promising modality that combines penetration depth, resolution, and functional information [33]. It enables real-time, high-resolution imaging of microvasculature, supporting research into neurovascular coupling, cardiovascular disease, and tissue metabolism. Ongoing advances in acquisition speed, spatial resolution, and data processing are expected to accelerate translation into clinical use [75]. Reported performance includes lateral resolutions as fine as ~2–3 μm in functional photoacoustic microscopy and up to ~120 μm in all-optical 3D tomography; axial resolutions from ~7 to ~100 μm; and imaging depths from several hundred micrometers (microscopy) to ~12 mm (tomography) [80]. Target vessel sizes range from capillaries (<20 μm) and cortical microvasculature (<50 μm) to larger vessels up to ~1 mm in diameter, enabling assessment of both microcirculatory and macrovascular structures [81]. Preclinical studies dominate current applications, including *in vivo* mouse brain functional imaging, vascular network mapping, oxygenation quantification, and cerebrovascular morphology analysis [76,82]. However, clinical-oriented investigations have already demonstrated feasibility for vascular imaging of human fingers and wrists, as well as *in vivo* 3D mapping of brain vasculature, highlighting potential for future use in vascular disease diagnosis and inflammation assessment [83].

Conclusion

This review has revisited the fundamental principles of Doppler ultrasound, from its historical origins to its modern applications in blood flow imaging. We've highlighted often-overlooked aspects of the Doppler spectrum, such as spectral broadening and amplitude, emphasizing their potential to provide deeper clinical insights into blood properties and hemodynamics. A comparative analysis of conventional modes, including PW, color, and power Doppler, alongside B-Flow imaging, underscored their respective strengths and limitations, while also addressing key sources of measurement uncertainty. Furthermore, we've explored the exciting frontier of vascular imaging. Recently commercialized technologies like contrast-free MVFI and real-time 3D vascular imaging are already enhancing diagnostic capabilities. Looking ahead, preclinical systems involving high-frame-rate imaging and PAI promise to revolutionize our ability to visualize microvascular networks and slow flow. By understanding both the foundational principles and these emerging technologies, clinicians and researchers can better leverage ultrasound to its full potential for the accurate diagnosis and monitoring of vascular conditions.

ORCID: Dong-Guk Paeng: https://orcid.org/0000-0001-5106-3747; Cheong-Ah Lee: https://orcid.org/0000-0002-4121-2857; Cynthia Imtiaz: https://orcid.org/0009-0002-9256-7110

Author Contributions

Conceptualization: Paeng DG. Data acquisition: Lee CA, Imtiaz C. Data analysis or interpretation: Paeng DG, Lee CA. Drafting of the manuscript: Paeng DG, Lee CA, Imtiaz C. Critical revision of the manuscript: Paeng DG. Approval of the final version of the manuscript: all authors.

Conflict of Interest

No potential conflict of interest relevant to this article was reported.

Acknowledgments

This work was supported by the research grant from the Chuongbong Academic Research Fund of Jeju National University in 2023.

References

1. Satomura S. Ultrasonic Doppler method for the inspection of cardiac functions. J Acoust Soc Am 1957;29:1181-1185.

2. Coman IM, Popescu BA. Shigeo Satomura: 60 years of Doppler ultrasound in medicine. Cardiovasc Ultrasound 2015;13:48.
3. Kato K, Kido Y, Motomiya M, Kaneko Z, Kotani H. On the mechanism of generation of detected sound in ultrasonic flowmeter. Mem Inst Sci Ind Res Osaka Univ 1962;19:51-57.
4. Flachskampf FA, Kohler J, Ask P, Lepper W, Hanrath P. Overestimation of flow velocity through leaks in mechanical valve prostheses and through small orifices by continuous-wave Doppler. J Am Soc Echocardiogr 1997;10:904-914.
5. Stamm RB, Martin RP. Quantification of pressure gradients across stenotic valves by Doppler ultrasound. J Am Coll Cardiol 1983;2:707-718.
6. Aziz MU, Eisenbrey JR, Deganello A, Zahid M, Sharbidre K, Sidhu P, et al. Microvascular flow imaging: a state-of-the-art review of clinical use and promise. Radiology 2022;305:250-264.
7. Kang HJ, Lee JM, Jeon SK, Ryu H, Yoo J, Lee JK, et al. Microvascular flow imaging of residual or recurrent hepatocellular carcinoma after transarterial chemoembolization: comparison with color/power Doppler imaging. Korean J Radiol 2019;20:1114-1123.
8. Huang H, Hsu PL, Tsai SF, Chuang YH, Chen DQ, Xu GX, et al. High-spatiotemporal-resolution ultrasound flow imaging to determine cerebrovascular hemodynamics in Alzheimer's disease mice model. Adv Sci (Weinh) 2023;10:e2302345.
9. Pakdaman Zangabad R, Iskander-Rizk S, van der Meulen P, Meijlink B, Kooiman K, Wang T, et al. Photoacoustic flow velocity imaging based on complex field decorrelation. Photoacoustics 2021;22:100256.
10. Hames TK, Humphries KN, Gazzard VM, Powell TV, McLellan DL. The role of continuous wave Doppler imaging in a vascular unit. Cardiovasc Res 1985;19:631-635.
11. Woo J. A short history of the development of diagnostic ultrasound in Japan (with reference to obstetrical and gynecological applications) [Internet]. The Author; 1998-2025 [cited 2025 Aug 1]. Available from: https://www.ob-ultrasound.net/japan_ultrasonics.html.
12. Paeng DG, Chiao RY, Shung KK. Echogenicity variations from porcine blood II: the "bright ring" under oscillatory flow. Ultrasound Med Biol 2004;30:815-825.
13. Franklin DL, Baker DW, Ellis RM, Rushmer RF. A pulsed ultrasonic flowmeter. IRE Trans Med Electron 1959;6:204-206.
14. Barber FE, Baker DW, Nation AW, Strandness DE Jr, Reid JM. Ultrasonic duplex echo-Doppler scanner. IEEE Trans Biomed Eng 1974;21:109-113.
15. Rubin JM, Bude RO, Carson PL, Bree RL, Adler RS. Power Doppler US: a potentially useful alternative to mean frequency-based color Doppler US. Radiology 1994;190:853-856.
16. Pooh RK. New application of B-flow sono-angiography in perinatology. Ultrasound Obstet Gynecol 2000;15:163.
17. Smith MD, Kwan OL, DeMaria AN. Value and limitations of continuous-wave Doppler echocardiography in estimating severity of valvular stenosis. JAMA 1986;255:3145-3151.
18. Lee J. Hemodynamics in Doppler ultrasonography. Ultrasonography 2024;43:413-423.
19. Burstow DJ, Nishimura RA, Bailey KR, Reeder GS, Holmes DR Jr, Seward JB, et al. Continuous wave Doppler echocardiographic measurement of prosthetic valve gradients: a simultaneous Doppler-catheter correlative study. Circulation 1989;80:504-514.
20. Martin RP. Clinical implementation of continuous-wave Doppler: it made all the difference. J Am Soc Echocardiogr 2018;31:1323-1329.
21. Nishimura RA, Callahan MJ, Schaff HV, Ilstrup DM, Miller FA, Tajik AJ. Noninvasive measurement of cardiac output by continuous-wave Doppler echocardiography: initial experience and review of the literature. Mayo Clin Proc 1984;59:484-489.
22. Sachpekidis V, Papadopoulou SL, Kantartzi V, Styliadis I, Nihoyannopoulos P. A novel handheld echocardiography device with continuous-wave Doppler capability: implications for the evaluation of aortic stenosis severity. J Am Soc Echocardiogr 2022;35:1273-1280.
23. Maslow A, Comunale ME, Haering JM, Watkins J. Pulsed wave Doppler measurement of cardiac output from the right ventricular outflow tract. Anesth Analg 1996;83:466-471.
24. Huntsman LL, Stewart DK, Barnes SR, Franklin SB, Colocousis JS, Hessel EA. Noninvasive Doppler determination of cardiac output in man: clinical validation. Circulation 1983;67:593-602.
25. Arbeille P, Bouin-Pineau MH, Herault S. Accuracy of the main Doppler methods for evaluating the degree of carotid stenoses (continuous wave, pulsed wave, and color Doppler). Ultrasound Med Biol 1999;25:65-73.
26. Grant EG, Benson CB, Moneta GL, Alexandrov AV, Baker JD, Bluth EI, et al. Carotid artery stenosis: gray-scale and Doppler US diagnosis: Society of Radiologists in Ultrasound Consensus Conference. Radiology 2003;229:340-346.
27. Villanueva FS, Gertz EW, Csikari M, Pulido G, Fisher D, Sklenar J. Detection of coronary artery stenosis with power Doppler imaging. Circulation 2001;103:2624-2630.
28. Oglat AA, Matjafri MZ, Suardi N, Oqlat MA, Abdelrahman MA, Oqlat AA. A Review of Medical Doppler ultrasonography of blood flow in general and especially in common carotid artery. J Med Ultrasound 2018;26:3-13.
29. Russ MK, Lafata NM, Robertson SH, Samei E. Pulsed wave Doppler ultrasound: accuracy, variability, and impact of acquisition parameters on flow measurements. Med Phys 2023;50:6704-6713.
30. Correia M, Provost J, Tanter M, Pernot M. 4D ultrafast ultrasound flow imaging: in vivo quantification of arterial volumetric flow rate in a single heartbeat. Phys Med Biol 2016;61:L48-L61.
31. Park B, Oh D, Kim J, Kim C. Functional photoacoustic imaging: from nano- and micro- to macro-scale. Nano Converg 2023;10:29.
32. Mirg S, Turner KL, Chen H, Drew PJ, Kothapalli SR. Photoacoustic

imaging for microcirculation. Microcirculation 2022;29:e12776.
33. Zhang Y, Hong H, Cai W. Photoacoustic imaging. Cold Spring Harb Protoc 2011;2011:10.1101/pdb.top065508 pdb.top065508.
34. Chen SY, Hsu HY. Analysis of Doppler blood flow waveform of cerebral arteries and common abnormal findings. J Med Ultrasound 2014;22:3-6.
35. Kim ES, Sharma AM, Scissons R, Dawson D, Eberhardt RT, Gerhard-Herman M, et al. Interpretation of peripheral arterial and venous Doppler waveforms: a consensus statement from the Society for Vascular Medicine and Society for vascular ultrasound. Vasc Med 2020;25:484-506.
36. Paeng DG, Chiao RY, Shung KK. Echogenicity variations from porcine blood I: the "bright collapsing ring" under pulsatile flow. Ultrasound Med Biol 2004;30:45-55.
37. Huang CC, Chou HL, Chen PY. Measurement of the Doppler power of flowing blood using ultrasound Doppler devices. Ultrasound Med Biol 2015;41:565-573.
38. Oppermann I, Hamalainen M, Iinatti J. UWB: theory and applications. Chichester: John Wiley & Sons, 2004.
39. Chaoui R, Kalache KD, Hartung J. Application of three-dimensional power Doppler ultrasound in prenatal diagnosis. Ultrasound Obstet Gynecol 2001;17:22-29.
40. Paeng DG, Nam KH, Choi MJ, Shung KK. Three-dimensional reconstruction of the "bright ring" echogenicity from porcine blood upstream in a stenosed tube. IEEE Trans Ultrason Ferroelectr Freq Control 2009;56:880-885.
41. Bascom PA, Cobbold RS. Origin of the Doppler ultrasound spectrum from blood. IEEE Trans Biomed Eng 1996;43:562-571.
42. Baechtiger R, Nyffeler F. 1985 Index IEEE Transactions on Sonics and Ultrasonics. IEEE Trans Sonics Ultrason 1985;32:866.
43. Yoo J, Je BK, Choo JY. Ultrasonographic demonstration of the tissue microvasculature in children: microvascular ultrasonography versus conventional color Doppler ultrasonography. Korean J Radiol 2020;21:146-158.
44. Kaunitz JD. The Doppler effect: a century from red shift to red spot. Dig Dis Sci 2016;61:340-341.
45. Pan FS, Yu L, Luo J, Wu RD, Xu M, Liang JY, et al. Carotid artery stiffness assessment by Ultrafast ultrasound imaging: feasibility and potential influencing factors. J Ultrasound Med 2018;37:2759-2767.
46. Smith E, Azzopardi C, Thaker S, Botchu R, Gupta H. Power Doppler in musculoskeletal ultrasound: uses, pitfalls and principles to overcome its shortcomings. J Ultrasound 2021;24:151-156.
47. Harloff A, Zech T, Wegent F, Strecker C, Weiller C, Markl M. Comparison of blood flow velocity quantification by 4D flow MR imaging with ultrasound at the carotid bifurcation. AJNR Am J Neuroradiol 2013;34:1407-1413.
48. Hua Y, Meng XF, Jia LY, Ling C, Miao ZR, Ling F, et al. Color Doppler imaging evaluation of proximal vertebral artery stenosis. AJR Am J Roentgenol 2009;193:1434-1438.
49. Cantisani V, Olive M, Di Segni M, Di Leo N, Grazdhani H, D'Ettorre G, et al. Contrast-enhanced ultrasonographic (CEUS) and elastosonographic features of a case of testicular Leydig tumor. Ultraschall Med 2012;33:409-410.
50. Bae JS, Lee JM, Jeon SK, Jang S. Comparison of MicroFlow Imaging with color and power Doppler imaging for detecting and characterizing blood flow signals in hepatocellular carcinoma. Ultrasonography 2020;39:85-93.
51. Almuhanna N, Wortsman X, Wohlmuth-Wieser I, Kinoshita-Ise M, Alhusayen R. Overview of ultrasound imaging applications in dermatology. J Cutan Med Surg 2021;25:521-529.
52. Gold L, Nazarian LN, Johar AS, Rao VM. Characterization of maxillofacial soft tissue vascular anomalies by ultrasound and color Doppler imaging: an adjuvant to computed tomography and magnetic resonance imaging. J Oral Maxillofac Surg 2003;61:19-31.
53. Filippucci E, Salaffi F, Carotti M, Grassi W. Doppler ultrasound imaging techniques for assessment of synovial inflammation. Rep Med Imaging 2013;6:83-91.
54. Yang J, Pang C, Song XD, Gao X. A method for gray-scale imaging of blood flow using high-frequency ultrasound. Ultrason Imaging 2018;40:3-14.
55. Park AY, Seo BK. Up-to-date Doppler techniques for breast tumor vascularity: superb microvascular imaging and contrast-enhanced ultrasound. Ultrasonography 2018;37:98-106.
56. Hofmann AG, Mlekusch I, Wickenhauser G, Assadian A, Taher F. Clinical applications of B-flow ultrasound: a scoping review of the literature. Diagnostics (Basel) 2023;13:397.
57. Lin JM, Huang GF, Xie QC, Lyu GR, Lin J, Huang SS, et al. Application of B-flow imaging and its enhanced mode in perforator mapping. Clin Radiol 2023;78:387-393.
58. Gudmundson E, Jakobsson A, Gran F. Overcoming the Nyquist limit in blood flow velocity estimation. In: 2012 IEEE International Ultrasonics Symposium (IUS'12); 2012 Oct 7-10; Dresden, Germany. Piscataway, NJ: Institute of Electrical and Electronics Engineers, 2012;1615-1618.
59. Du Y, Ding H, He L, Yiu BYS, Deng L, Yu AC, et al. Quantitative blood flow measurements in the common carotid artery: a comparative study of high-frame-rate ultrasound vector flow imaging, pulsed wave Doppler, and phase contrast magnetic resonance imaging. Diagnostics (Basel) 2022;12:690.
60. Lurie F, Pevec WC. Ultrasound estimates of venous valve function in screening for insufficiency and following patients with chronic venous disease. Int J Angiol 2000;9:246-249.
61. Fogarty P, Beattie B, Harper A, Dornan J. Continuous wave Doppler flow velocity waveforms from the umbilical artery in normal pregnancy. J Perinat Med 1990;18:51-57.
62. Arduini D, Rizzo G, Mancuso S, Romanini C. Longitudinal

assessment of blood flow velocity waveforms in the healthy human fetus. Prenat Diagn 1987;7:613-617.
63. Jensen JA, Lacasa IR. Estimation of blood velocity vectors using transverse ultrasound beam focusing and cross-correlation. In: 1999 IEEE Ultrasonics Symposium (Cat. No. 99CH37027); 1999 Oct 17-20; Tahoe, NV, USA. Piscataway, NJ: Institute of Electrical and Electronics Engineers, 1999;1493-1497.
64. Eberhardt RT, Raffetto JD. Chronic venous insufficiency. Circulation 2014;130:333-346.
65. Artul S, Nseir W, Armaly Z, Soudack M. Superb microvascular imaging: added value and novel applications. J Clin Imaging Sci 2017;7:45.
66. Frijlingh M, Stoelinga B, de Leeuw RA, Hehenkamp WJ, Twisk JW, van den Bosch T, et al. Microvascular flow imaging of fibroids: a prospective pilot study. Acta Obstet Gynecol Scand 2024;103:2193-2202.
67. Amin Naji M, Panduro NS, Tabatabaei Majd SM, Hansen LN, Taghavi I, McDermott A, et al. Human lymph node microvascular imaging using a fast contrast-free super-resolution ultrasound technique. Sci Rep 2025;15:23061.
68. Heiles B, Correia M, Hingot V, Pernot M, Provost J, Tanter M, et al. Ultrafast 3D ultrasound localization microscopy using a 32 x 32 matrix array. IEEE Trans Med Imaging 2019;38:2005-2015.
69. Haniel J, Yiu BY, Chee AJ, Huebner R, Yu AC. Efficacy of ultrasound vector flow imaging in tracking omnidirectional pulsatile flow. Med Phys 2023;50:1699-1714.
70. Gesnik M, Blaize K, Deffieux T, Gennisson JL, Sahel JA, Fink M, et al. 3D functional ultrasound imaging of the cerebral visual system in rodents. Neuroimage 2017;149:267-274.
71. Jensen JA, Schou M, Jorgensen LT, Tomov BG, Stuart MB, Traberg MS, et al. anatomic and functional imaging using row-column arrays. IEEE Trans Ultrason Ferroelectr Freq Control 2022;69:2722-2738.
72. Caudoux M, Demeulenaere O, Poree J, Sauvage J, Mateo P, Ghaleb B, et al. Curved toroidal row column addressed transducer for 3D Ultrafast ultrasound imaging. IEEE Trans Med Imaging 2024;43:3279-3291.
73. Hansen-Shearer J, Yan J, Lerendegui M, Huang B, Toulemonde M, Riemer K, et al. Ultrafast 3-D transcutaneous super resolution ultrasound using row-column array specific coherence-based beamforming and rolling acoustic sub-aperture processing: in vitro, in rabbit and in human study. Ultrasound Med Biol 2024;50:1045-1057.
74. Errico C, Pierre J, Pezet S, Desailly Y, Lenkei Z, Couture O, et al. Ultrafast ultrasound localization microscopy for deep super-resolution vascular imaging. Nature 2015;527:499-502.
75. Yao J, Wang LV. Sensitivity of photoacoustic microscopy. Photoacoustics 2014;2:87-101.
76. Wang Z, Ai C, Sun T, Wang Z, Zhang W, Zhou F, et al. Photoacoustic imaging detects cerebrovascular pathological changes in sepsis. Photoacoustics 2025;44:100737.
77. Sweeney PW, Hacker L, Lefebvre TL, Brown EL, Grohl J, Bohndiek SE. Unsupervised segmentation of 3D microvascular photoacoustic images using deep generative learning. Adv Sci (Weinh) 2024;11:e2402195.
78. Foiret J, Zhang H, Ilovitsh T, Mahakian L, Tam S, Ferrara KW. Ultrasound localization microscopy to image and assess microvasculature in a rat kidney. Sci Rep 2017;7:13662.
79. Chen Y, Chen B, Yu T, Yin L, Sun M, He W, et al. Photoacoustic mouse brain imaging using an optical Fabry-Perot interferometric ultrasound sensor. Front Neurosci 2021;15:672788.
80. Yao J, Wang L, Yang JM, Maslov KI, Wong TT, Li L, et al. High-speed label-free functional photoacoustic microscopy of mouse brain in action. Nat Methods 2015;12:407-410.
81. Nasiriavanaki M, Xia J, Wan H, Bauer AQ, Culver JP, Wang LV. High-resolution photoacoustic tomography of resting-state functional connectivity in the mouse brain. Proc Natl Acad Sci U S A 2014;111:21-26.
82. Wang Q, Shi Y. Photoacoustic viscoelasticity imaging for the detection of acute hepatitis: a feasibility study. Biophys Rep 2020;6:1-8.
83. Yao J, Huang CH, Wang L, Yang JM, Gao L, Maslov KI, et al. Wide-field fast-scanning photoacoustic microscopy based on a water-immersible MEMS scanning mirror. J Biomed Opt 2012;17:080505-080501.